ACS Catalysis

Research Article

pubs.acs.org/acscatalysis

Fabrication of Hierarchically Porous RuO_2–CuO/Al–ZrO_2 Composite as Highly Efficient Catalyst for Ammonia-Selective Catalytic Oxidation

Xiangzhi Cui,[†] Lisong Chen,[†] Yongxia Wang,[†] Hangrong Chen,[†] Wenru Zhao,[‡] Yongsheng Li,[‡] and Jianlin Shi*,[†]

[†]The State Key Laboratory of High Performance Ceramics and Superfine Microstructures, Shanghai Institute of Ceramics, Chinese Academy of Sciences, Shanghai 200050, People's Republic of China

[‡]Key Laboratory for Ultrafine Materials of Ministry of Education, School of Materials Science and Engineering, East China University of Science and Technology, Shanghai 200237, People's Republic of China

Supporting Information

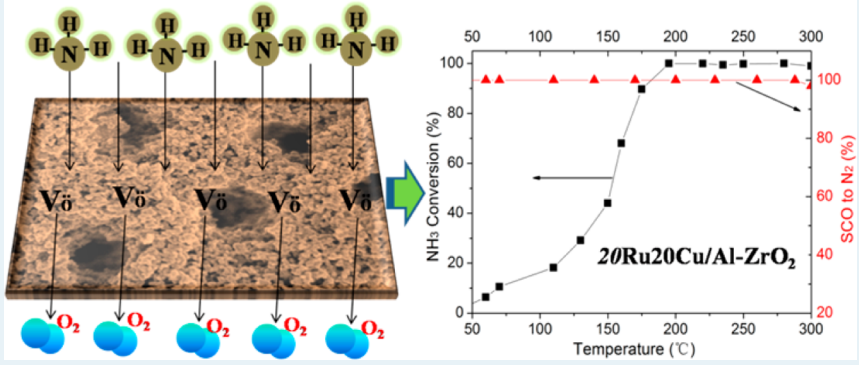

ABSTRACT: A hierarchically porous RuO_2–CuO/(Al–ZrO_2) nanocomposite, with RuO_2 and CuO nanocrystals being homogeneously dispersed in the hierarchically porous structure of Al-doped ZrO_2 (Al–ZrO_2), has been developed by a hydrothermal and wet impregnation method for efficient ammonia-selective catalytic oxidation (SCO) applications. The microstructures of the RuO_2–CuO/Al–ZrO_2 nanocomposites were characterized by XRD, TEM, FESEM, EDX elemental mapping, and N_2 sorption. XPS analysis and H_2-TPR results indicate that the hierarchically porous RuO_2–CuO/Al–ZrO_2 composites possess a large number of oxygen vacancies and surface catalytic active sites, which endows the composite with high catalytic activity and N_2 selectivity for NH_3 oxidation. NH_3 complete oxidization has been achieved at 195 °C with 100% N_2 selectivity over an obtained RuO_2–CuO/Al–ZrO_2 composite at RuO/CuO = 1:1 (weight rate). The high efficiency of hierarchically porous RuO_2–CuO/Al–ZrO_2 nanocomposites for ammonia SCO reaction has been attributed to the synergetic catalytic effects among the metal oxides, in which the porous Al–ZrO_2 support promotes oxygen activation by the generation of oxygen vacancies due to the Al doping, and the ultrahigh catalytic activity of RuO_2 is responsible for the active NH_3 oxidation. Successively, CuO plays a role of NO intermediate conversion for enhanced N_2 selectivity.

KEYWORDS: *hierarchically porous, RuO_2–CuO/Al–ZrO_2, NH_3, selective catalytic oxidation, nanocomposites, synergetic catalysis*

1. INTRODUCTION

Ammonia (NH_3) is one of the most common gaseous pollutants in the human environment, and the removal of NH_3 has become a very important environmental issue. Many kinds of chemical technologies have been adopted for NH_3 removal, including adsorption, absorption, chemical treatment, catalytic decomposition, selective catalytic oxidation (SCO), etc.,[1−3] although the SCO of NH_3 to N_2 and H_2O is regarded as one of the best potential approaches nowadays for effectively removing NH_3 from oxygen-containing waste gases.

Various kinds of materials have been reported to be useful catalysts for ammonia SCO reaction in the past few years. First, noble-metal-based catalysts have been developed for the SCO reaction, including Pd,[4] Pt,[5] Au,[6] Ag,[7] RuO_2,[8] etc., which are very active for catalytic oxidation of NH_3 and can completely oxidize NH_3 at low temperatures (200−350 °C). Unfortunately, selectivities of NH_3 oxidation to N_2 on these noble-metal-based catalysts are relatively low (typically ≤80%). In addition, many kinds of transition-metal-oxide catalysts have been reported to be active for SCO of NH_3, such as V_2O_5,[9] CoO_3,[10] Fe_2O_3,[11] CuO,[12] MoO_3,[13] MnO_2,[14] CeO_2,[15] and TiO_2.[16−18] The N_2 selectivity of these transition metal oxide

Received: March 30, 2014
Revised: May 9, 2014
Published: May 23, 2014

   dx.doi.org/10.1021/cs500421x | ACS Catal. 2014, 4, 2195−2206

catalysts was enhanced as compared with the noble metal catalyst; however, they need significantly higher operation temperatures (300−500 °C) than the latter. Among the SCO catalysts, a V_2O_5/TiO_2 catalyst reported by Li and Armor[9] was quite selective for N_2 at T < 300 °C; however, the toxicity of V_2O_5 prohibits wide application of the V_2O_5/TiO_2 catalyst in large-scale chemical factories. Huang[19] prepared an activated carbon fiber (ACF)-supported copper catalyst and reported that the obtained catalyst showed 95−97% NH_3 conversion and 97−100% N_2 selectivity for the ammonia SCO reaction, which should be an attractive catalyst for NH_3 removal. However, the stability or durability of long-term use of ACF for oxidizing in the atmosphere during the O_2-rich NH_3 oxidation reaction are the main concerns and should be further verified. As a whole, it is still a great challenge to achieve both complete NH_3 conversion at relatively low temperature and high N_2 selectivity of NH_3 oxidation by using low cost, long-lasting, and environmentally friendly catalysts.

Ruthenium oxide (RuO_2) has been reported to be very active for NH_3 oxidation, especially on the RuO_2 (110) surface, which shows high catalytic ability for oxidation reactions of NH_3,[8,20−24] HCl,[25,26] and CO.[27,28] In 2005, Wang et al.[20] showed that a single-crystal RuO_2 (110) surface exhibits high catalytic activity for NH_3 oxidation under ultrahigh vacuum (UHV). In our previous work,[23] we reported that NH_3 can be oxidized completely at 180 °C on mesostructured Cu−Ru bimetal oxides with high N_2 selectivity (>95%). Unfortunately, the amount of RuO_2 used in the mesostructured Ru−Cu bimetal oxide is high (RuO_2/CuO = 9:1, weight rate), which is undesirable for developing low cost and environmentally friendly catalysts.

Zirconia is an interesting functional catalytic material because of the presence of both acidic centers and basic centers on its surface and its high ion exchange capability, and therefore, it has been used widely in catalysis fields.[29−32] Wang et al.[15] demonstrated that the addition of Zr to ceria could lead to a phase transition and the generation of oxygen vacancies over ceria−zirconia mixed catalysts, and this catalyst showed excellent NH_3 oxidation activity at ∼360 °C.

It has been widely reported that the catalytic activity can be much enhanced on porous-structured catalyst with a high surface area, and the acidity of a catalyst component, such as zirconia or alumina, should be effective for alkali-involved reactions, such as the NH_3 oxidation reaction. In this work, we designed and prepared hierarchically porous aluminum-doped zirconia (Al−ZrO_2) by a hydrothermal method, and then RuO_2 and CuO nanoparticles were loaded by a post impregnation method. The obtained hierarchically porous RuO_2−CuO/Al−ZrO_2 composite with RuO_2/CuO = 1 (weight rate) showed high catalytic activity for the NH_3 SCO reaction with complete NH_3 conversion at 195 °C and N_2 selectivity of 100%. This should be attributed to the synergetic catalytic effects among the metal oxides, in which the Al−ZrO_2 support is responsible for the O_2 molecule's adsorption and activation to active oxygen species O* at the oxygen vacancies on the porous matrix. Then the RuO_2 component catalyzes the oxidation and dehydrogenation of adsorbed $NH_{3\text{-cus}}$ species on its surface, followed by the reduction conversion of the intermediate, such as NO, during NH_3 oxidization into N_2 by the CuO component.

2. EXPERIMENTAL SECTION

2.1. Chemicals and Reagents. Brij35 ($CH_3(CH_2)_{10}CH_2(OCH_2CH_2)_{23}OH$) and Zr-($OCH_2CH_2CH_3)_4$ were obtained from Shanghai J&K, China. P123 ($EO_{20}PO_{70}EO_{20}$) was obtained from SIGMA.

2.2. Materials Synthesis. *2.2.1. Synthesis of Hierarchically Porous Al−ZrO_2.* Hierarchically porous Al-doped zirconia was synthesized by the hydrothermal method using P123 and Brij35 as surface active agents. Typically, 3.7 g of P123 and 4.5 g of Brij35 were dissolved into 100 mL of deionized water, and then $AlCl_3{\cdot}6H_2O$ was added into the solution by stirring until the complete dissolution of $AlCl_3{\cdot}6H_2O$. After that, 10 mL $Zr(OCH_2CH_2CH_3)_4$ was added dropwise slowly under stirring, and the obtained solution with Zr/Al = 10:1 (atom rate) was continuously stirred for another 12 h, then the solution was poured into an autoclave for hydrothermal reaction at 80 °C for 24 h. The obtained white product was placed into ethanol at 80 °C for 6 h to extract surface agents and named as Al−ZrO_2. For comparison, hierarchically porous undoped zirconia was also synthesized by the same procedure and named as ZrO_2.

2.2.2. Preparation of Hierarchically Porous CuO/Al−ZrO_2 Composites. CuO nanoparticles were loaded on the hierarchically porous Al−ZrO_2 by a wet impregnation method. First, a solution of Cu(II) nitrate was prepared by dissolving $Cu(NO_3)_2{\cdot}3H_2O$ in 5 mL of ethanol, and then the ethanol precursor solutions was impregnated into 0.5 g of prepared Al−ZrO_2. The composite $Cu(NO_3)_2$@Al−ZrO_2 was obtained after the evaporation of ethanol, and then the composite was calcined at 550 °C to form hierarchically porous CuO/Al−ZrO_2 nanocomposites and named as XCu/Al−ZrO_2, in which X (weight percentage) was varied from 5 to 30.

2.2.3. Preparation of Hierarchically Porous RuO_2CuO/Al−ZrO_2 Composites. RuO_2 and CuO nanoparticles were coloaded on the hierarchically porous Al−ZrO_2 by the same wet impregnation method mentioned above. First, a mixed solution of Cu(II) nitrate and Ru(III) chloride (total 2 g) was prepared by dissolving $Cu(NO_3)_2{\cdot}3H_2O$ and $RuCl_3$ in 5 mL of ethanol. The weight percentag, X, of Ru(IV) oxide (RuO_2) in the metal oxides, $X = ([RuO_2]/([RuO_2] + [CuO] + [Al{-}ZrO_2])) \times 100$, was varied from 5 to 30, and the content of Cu(II) oxide (CuO) was kept at a constant value of 20 wt %. The prepared hierarchically porous composites were named as XRu20Cu/Al−ZrO_2. A reference sample with 20 wt % RuO_2-loaded Al−ZrO_2 was also prepared following the same method and named as 20Ru/Al−ZrO_2.

For comparison, CuO and RuO_2 nanoparticles loaded on the hierarchically porous ZrO_2 were also synthesized by the same wet impregnation method mentioned above and named 20Cu/Al−ZrO_2 and 20Ru20Cu/Al−ZrO_2 according to the loading amount of CuO (20 wt %) and RuO_2 (20 wt %), respectively.

2.3. Structural Characterizations. The powder X-ray diffraction (XRD) patterns of prepared samples were recorded on a Rigaku D/Max-2550 V X-ray diffractometer with a Cu Kα radiation target (40 kV, 40 mA). The N_2 sorption measurements were performed using Micromeritics Tristar 3000 at 77 K, and the specific surface area and the pore size distribution were calculated using the Brunauer−Emmett−Teller (BET) and Barrett−Joyner−Halenda (BJH) methods, respectively. Field emission scanning electron microscopic (FE-SEM) images were performed on a JEOL JSM-6700F field emission scanning electron microscopy. Transmission electron microscopy (TEM) images and energy-dispersive X-ray spectra

dx.doi.org/10.1021/cs500421x | ACS Catal. 2014, 4, 2195−2206

(EDX) were obtained on a JEOL 200CX electron microscope operating at 160 kV. X-ray photoelectron spectroscopic (XPS) analyses were carried out on a Microlab310-F Scanning Auger Microprobe equipped with a 150 W (15 kV by 10 mA) aluminum Kα (1486.6 eV) anode as the X-ray source, using a pass energy of 50 eV with a step size of 0.1 eV.

2.4. Hydrogen Temperature-Programmed Reduction. H_2 temperature-programmed reduction (H_2-TPR) profiles of composites were recorded on a TP-5080 auto multifunctional adsorption instrument at the atmospheric pressure . Typically, 50 mg of catalysts was placed in a quartz glass tube reactor to be pretreated at 100 °C for 30 min under flowing N_2 and then cooled to room temperature. Afterward, the 10% H_2 in Ar (30 mL min^{-1}) was introduced into the glass tube and thermally treated from room temperature to 700 °C at 10 °C min^{-1}, and the signal was recorded by TCD.

2.5. NH_3 Catalytic Oxidation Test. The activities of the catalysts for NH_3 oxidation were measured by a temperature-programmed reaction under atmospheric pressure in a fixed-bed quartz tubular reactor by using a thermal conductivity detector (TCD) of a gas chromatograph (GC-2060 system) equipped with a stainless-steel column (Porapak Q 80/80−100 mesh). The concentrations of NO, NO_2, and N_2O in the outlet gases were monitored continuously online by a NO_x analyzer (Thermo Fisher 42i-LS). No pretreatment was applied before each catalytic test. The composition of the reactant gases was fixed at 400 ppm of NH_3, 5% O_2, 6% moisture, and balanced with N_2. The moisture (water vapor) was introduced into the inlet gases by the thermostatic water bath at 100 °C. The reaction was conducted under a total flow rate of 200 sccm, a space velocity of 120 000 mL h^{-1} g_{cat}^{-1}. Typically, 0.1 g of catalyst was placed into the reaction tube and thermally treated from room temperature to 480 °C at 5 °C min^{-1}. The activity was expressed in the conversion rate of NH_3, and the intrinsic reaction rate (turnover frequency, TOF) was defined as the number of molecules of NH_3 reacted per mass catalyst per second (N_{NH_3} g_{cat}^{-1} s^{-1}) at a constant temperature of 150 °C.

When the SCO reaction reached a steady state, the NH_3 conversion and N_2 yield were calculated from the concentrations of the gases according to eqs 1 and 2.

$$\text{NH}_3\ \text{conversion}\ (\%) = \left(\frac{[\text{NH}_3]_{\text{in}} - [\text{NH}_3]_{\text{out}}}{[\text{NH}_3]_{\text{in}}}\right) \times 100 \quad (1)$$

$$\text{N}_2\ \text{yield}\ (\%) = \left(\frac{[\text{NH}_3]_{\text{in}} - [\text{NH}_3]_{\text{out}} - [\text{NO}]_{\text{out}} - [\text{NO}_2]_{\text{out}} - 2[\text{N}_2\text{O}]_{\text{out}}}{[\text{NH}_3]_{\text{in}}}\right) \times 100 \quad (2)$$

3. RESULTS

3.1. Structure Analyses. Figure 1 gives the XRD patterns of the prepared samples, and Al−ZrO_2 is well-crystallized in a tetragonal phase (JCPDS 50-1809). The copper oxide [Cu(II)] characteristic diffraction peaks (JCPDS 65-2309) become stronger at the increased CuO contents in *X*Cu/Al−ZrO_2 composites (Figure 1A). It also can be seen that the characteristic diffraction peaks of ruthenium oxide (RuO_2) are discerned for sample 5Ru20Cu/Al−ZrO_2 and become stronger with the increase in the RuO_2 addition amount (Figure 1B).

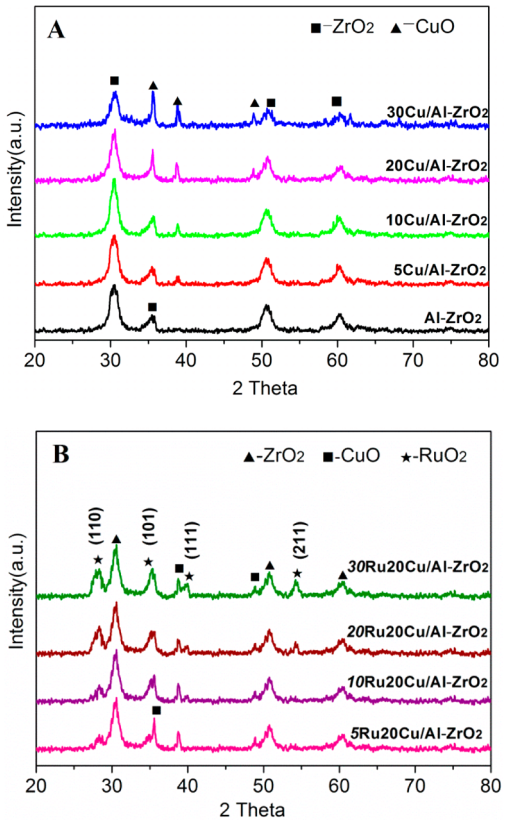

Figure 1. XRD patterns of prepared *X*Cu/Al−ZrO_2 composites (A) and *X*Ru20Cu/Al−ZrO_2 composites (B).

Moreover, the diffraction peaks of (110), (101), (111), and (211) lattice planes of RuO_2 at 2θ values of 28, 35, 40, and 54.5°, respectively, can also be observed in the samples 20Ru20Cu/Al−ZrO_2 and 30Ru20Cu/Al−ZrO_2 according to JCPDS 43-1027. This indicates that the crystalline zirconia doped with aluminum can be successfully synthesized by the hydrothermal and postcalcination method, and crystalline CuO and RuO_2 nanoparticles have been loaded into/onto the Al−ZrO_2 matrix. The zirconia reference samples without Al doping, 20Cu/ZrO_2 and 20Ru20Cu/ZrO_2, show crystal structure at the same calcination temperature (Supporting Information (SI) Figure S1).

All of the *X*Ru20Cu/Al−ZrO_2 samples exhibit similar isotherm curves with a IV hysteresis loop according to the nitrogen sorption isotherms in Figure 2A, and the hierarchically porous structure can be found from the pore size distribution curves (Figure 2B), in which the pore size peaks at about 5 and 30 nm can be seen, similar to the cases of the CuO particle-loaded Al−ZrO_2 composites (SI Figure S2). This indicates that the prepared *X*Ru20Cu/Al−ZrO_2 composites have hierarchically porous structure. The specific surface area data of these samples together with the corresponding pore sizes and pore volumes are summarized in Table 1. The obtained hierarchically porous composites possess relatively high surface areas of 111−335 m^2 g^{-1}, and the surface area and pore volume decrease gradually with the increasing CuO and RuO_2 loading amounts.

Typical FE-SEM images of the prepared oxide composites are shown in Figure 3. The pore diameters of 4−180 nm could be observed from the SEM images of Al−ZrO_2 (Figure 3A) and 20Cu/Al−ZrO_2 (Figure 3B), and the CuO nanoparticles are

dx.doi.org/10.1021/cs500421x | ACS Catal. 2014, 4, 2195−2206

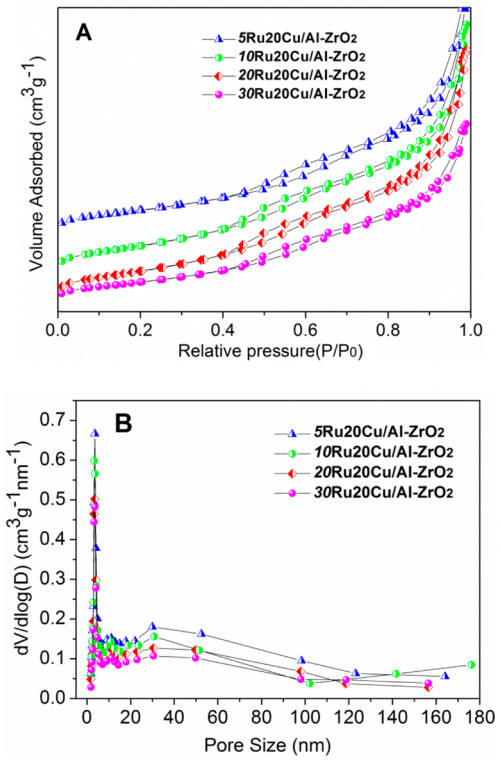

Figure 2. Nitrogen sorption isotherms of samples RuCu/Al−ZrO_2 (A) and the corresponding pore-size distribution curves (B).

dispersed homogeneously in the hierarchical pore structure of Al−ZrO_2 according to the EDX spectrum (Figure 3E) and the elemental mappings (B1 and B2) in the insets of Figure 3E. Moreover, the hierarchical pore structure is still retained after RuO_2 nanoparticles being loaded according to the images of 10Ru20Cu/Al−ZrO_2 (Figure 3C) and 20Ru20Cu/Al−ZrO_2 (Figure 3D), and it can also be seen from the EDX spectrum (Figure 3F) and the elemental mappings (D1 and D2) in the insets of Figure 3F that the CuO and RuO_2 nanoparticles are well-dispersed in the hierarchical pore structure of Al−ZrO_2, although the large pores become smaller for the sample loaded with 20 wt % RuO_2 (Figure 3D). The hierarchical pore structure of reference samples can also be found in SI Figure S3.

The representative TEM image in Figure 4A demonstrates the worm-like pore structure of the obtained Al−ZrO_2 composite as well as the reference samples (SI Figure S4), and the hierarchically porous structure of 20Cu/Al−ZrO_2 (Figure 4B), 10Ru20Cu/Al−ZrO_2 (Figure 4C), 20Ru20Cu/Al−ZrO_2 (Figure 4D), and 30Ru20Cu/Al−ZrO_2 (the inset in Figure 4E) is still retained, even though loaded with CuO and RuO_2 nanoparticles. From the high-resolution TEM image (Figure 4E), the lattice fringes can be clearly identified, and the smaller one of d = 0.26 nm could be attributed to the lattice (d = 0.256 nm, JCPDS 48-1548) plane of CuO particles, and the one of d = 0.32 nm can be indexed to the lattice (d = 0.318 nm, JCPDS 43-1027) plane of RuO_2. This further indicates the homogeneous dispersion of CuO and RuO_2 nanoparticles in the hierarchical pore structure of Al−ZrO_2. The corresponding selective area electron diffraction (SAED) in the inset of Figure 4E gives a ring-broadened diffraction pattern of polycrystalline structure, indicating the nanocrystalline feature of the hierarchically porous 20Ru20Cu/Al−ZrO_2 composite.

3.2. Catalytic Activity for Ammonia SCO. *3.2.1. Catalytic Activity for NH_3 Oxidation.* The catalytic activities of the prepared hierarchically porous composites for NH_3 oxidation are shown in Figure 5, and Table 1 gives the corresponding TOF values of the composite catalysts. Sample 20Cu/Al−ZrO_2 showes the highest catalytic activity for NH_3 oxidation reaction among the XCu/Al−ZrO_2 composites, with a TOF of 2.55 × 10^{16} N_{NH_3} g_{cat}^{-1} s^{-1} (the inset in Figure 6) and complete NH_3 oxidation temperature of 380 °C, as shown in the inset in Figure 5A. After coloading CuO and RuO_2 nanoparticles in the hierarchical pore structure of Al−ZrO_2, the catalytic activity for NH_3 oxidation is much enhanced (Figure 5B), and the TOF values increase significantly from the plot in Figure 6. NH_3 can be completely oxidized at 195 °C on composite 20Ru20Cu/Al−ZrO_2 (the inset in Figure 5B), with its highest TOF value of 2.03 × 10^{17} N_{NH_3} g_{cat}^{-1} s^{-1}, which is an order higher than that of 20Cu/Al−ZrO_2 (2.55 × 10^{16} N_{NH_3} g_{cat}^{-1} s^{-1}). Keeping at the same CuO addition amount (20 wt %), a lower or higher RuO_2 loading amount than 20 wt % will lead to a decreased catalytic activity of the composites, as shown from the TOF curve

Table 1. Pore Structural Parameters of Hierarchical Composites, And Their TOF Values for NH_3 Conversion at 150 °C and the Selectivity to N_2

sample	S_{BET}[a]/m^2 g^{-1}	D_{BJH}[b]/nm	V_{BJH}[c]/cm^3 g^{-1}	TOF[d]/N_{NH_3} g_{cat}^{-1} s^{-1}	SCO to N_2[e]/%
Al−ZrO_2	357	8.0	0.50		
5Cu/Al−ZrO_2	335	7.7	0.46	1.80 × 10^{16}	41
10Cu/Al−lZrO_2	308	7.6	0.34	2.25 × 10^{16}	60
20Cu/Al−lZrO_2	285	7.3	0.26	2.55 × 10^{16}	70
30Cu/Al−lZrO_2	205	7.2	0.30	2.70 × 10^{16}	60
5Ru20Cu/Al−lZrO_2	281	6.9	0.29	2.70 × 10^{16}	88
10Ru20Cu/Al−lZrO_2	282	6.7	0.24	5.40 × 10^{16}	99
20Ru20Cu/Al−lZrO_2	165	6.5	0.22	2.03 × 10^{17}	100
30Ru20Cu/Al−lZrO_2	111	6.2	0.16	9.45 × 10^{16}	100
20Ru/Al−lZrO_2	160	6.8	0.20		82
ZrO_2	228	5.1	0.47		
20Cu/ZrO_2	192	8.0	0.24		50
20Ru20Cu/ZrO_2	187	9.3	0.23		100

[a]BET surface area. [b]BJH desorption average pore diameter. [c]BJH desorption cumulative pore volume. [d]The number of NH_3 molecules of reacted per mass catalyst per second (N_{NH_3} g_{cat}^{-1} s^{-1}), the selectivity of N_2 for NH_3 complete oxidation. [e]The selectivity of N_2 for NH_3 complete oxidation.

dx.doi.org/10.1021/cs500421x | ACS Catal. 2014, 4, 2195−2206

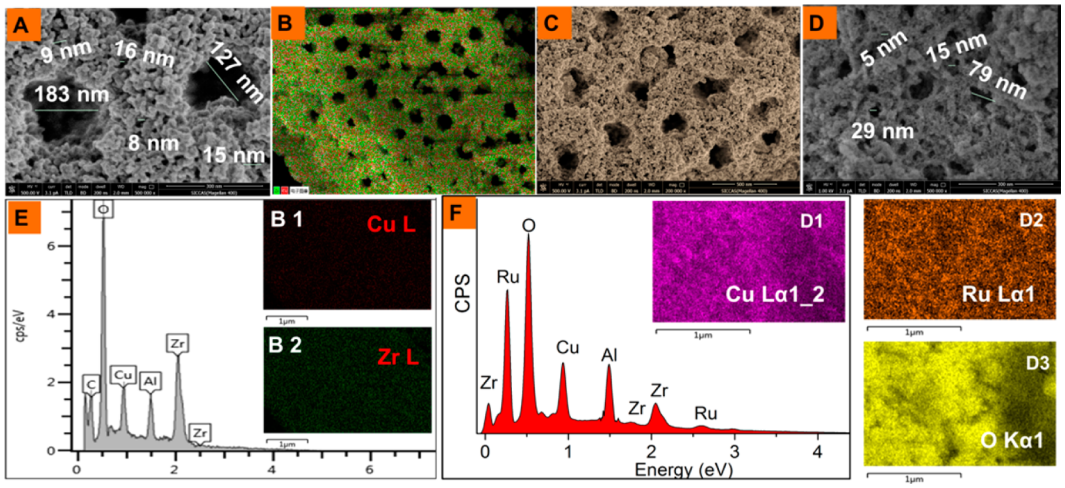

Figure 3. SEM images of hierarchically porous composites, (A) Al−ZrO_2, (B) 20Cu/Al−ZrO_2, (C) 10Ru20Cu/Al−ZrO_2, and (D) 20Ru20Cu/Al−ZrO_2. (E, F) EDX spectra of 20Cu/Al−ZrO_2 and 20Ru20Cu/Al−ZrO_2, respectively. B1 and B2 are the element mapping of image B, D1 ∼ D3 are the element mappings of image D.

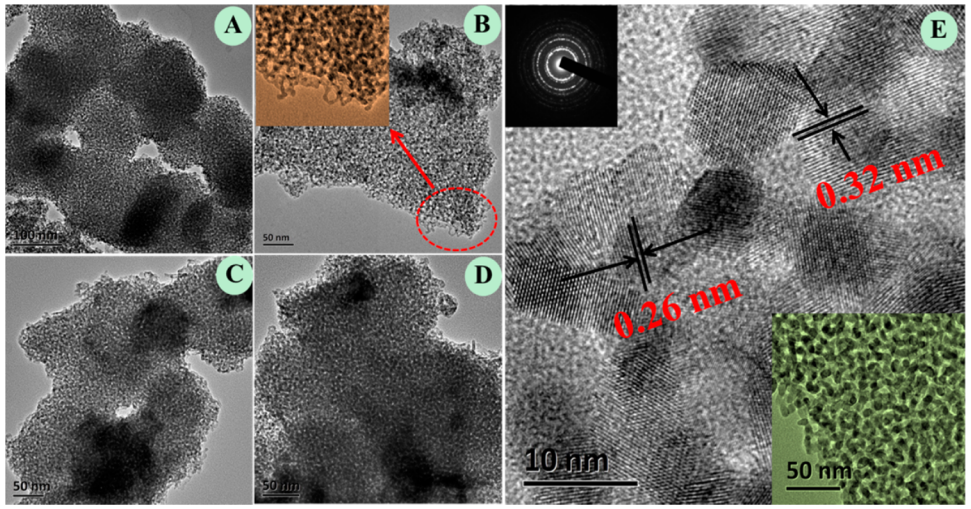

Figure 4. TEM images of the prepared hierarchically porous composites (A) Al−ZrO_2, (B) 20Cu/Al−ZrO_2, (C) 10Ru20Cu/Al−ZrO_2, (D) 30Ru20Cu/Al−ZrO_2, and the lower-right inset in (E) 20Ru20Cu/Al−ZrO_2. Inset in part B is an enlargement of the circled area. High-resolution TEM image (E) of sample 20Ru20Cu/Al−ZrO_2 and its SAED pattern in the upper-left inset.

(Figure 6) and the corresponding data in Table 1, as well as the NH_3 complete conversion temperatures (insets in Figure 5B). The weight ratio of 1:1 between loaded RuO_2 and CuO in hierarchically porous Al−ZrO_2 should be the optimum in the present case for the NH_3 oxidation reaction at low temperature. In addition, the hierarchical pore structure and the high surface area also contribute to the high catalytic activity of the composites for NH_3 SCO reaction.

3.2.2. N_2 Selectivity. The N_2 selectivity plots of the composite catalysts for NH_3 oxidation are shown in Figure 7, and Table 1 gives the N_2 selectivity data for complete oxidation of NH_3. For the *X*Cu/Al−ZrO_2 composite catalysts, the N_2 selectivity for NH_3 oxidation is above 90% when the reaction temperature is below 300 °C (Figure 7A), whereas it is lower than 70% when the NH_3 is completely oxidized at 400 °C (Table 1). After RuO_2 and CuO nanoparticles are coloaded in the hierarchical pore structure of Al−ZrO_2, the N_2 selectivity reaches ≥95%, and NH_3 can be 100% selectively oxidized to N_2 on catalyst 20Ru20Cu/Al−ZrO_2 at a wide range of temperatures (195−300 °C) (Figure 7B). The enhanced performance for 20Ru20Cu/Al−ZrO_2 for ammonia SCO should be due to the cooperative effects among RuO_2, CuO, and hierarchically porous Al−ZrO_2 nanoparticles. Although increasing the RuO_2 loading amount has little effect on the N_2 selectivity of *X*Ru20Cu/Al−ZrO_2 composite catalysts on ammonia SCO at lower than 300 °C, RuO_2 addition can significantly enhance the catalytic activity for NH_3 oxidation reaction below 300 °C (Figure 5).

From the data in SI Table S1 for comparison, the NH_3 complete conversion temperature of 20Ru20Cu/Al−ZrO_2 (195 °C) is 15 °C higher than previously reported mesostructured 10 wt % CuO/RuO_2 (180 °C),[23] whereas the RuO_2 use amount is much lower than the latter (CuO/RuO_2 = 1:9, weight rate). As for the conventional catalyst V_2O_5/TiO_2,[9] the N_2 selectivity was reported to be 89% at 400 °C with a 69% NH_3 conversion rate. Both the catalytic activity and selectivity are much lower than those of the hierarchically porous 20Ru20Cu/Al−ZrO_2. On the other hand, the surface area of hierarchically porous 20Ru20Cu/Al−ZrO_2 (165 m^2 g^{-1}) is much higher than that of mesostructured 10 wt % CuO/RuO_2

dx.doi.org/10.1021/cs500421x | *ACS Catal.* 2014, 4, 2195−2206

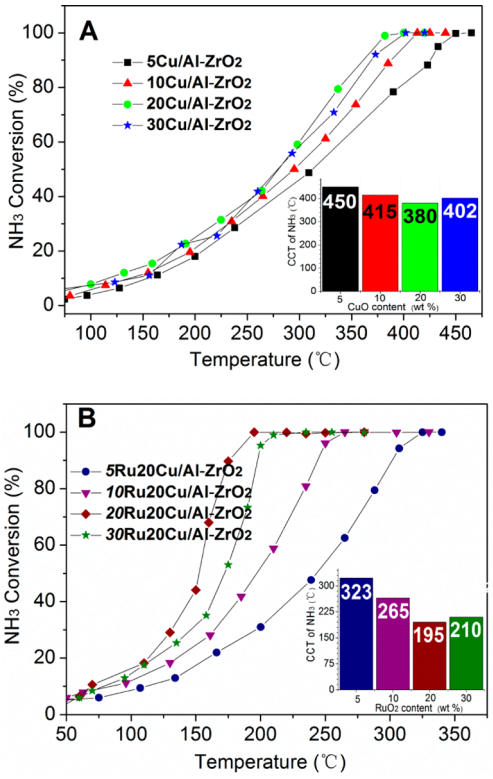

Figure 5. NH_3 conversion rate as a function of reaction temperature for hierarchical pore Cu/Al−ZrO_2 composites (A) and RuCu/Al−ZrO_2 composites (B). The inset histograms are the corresponding NH_3 complete conversion temperatures over the hierarchical pore composites.

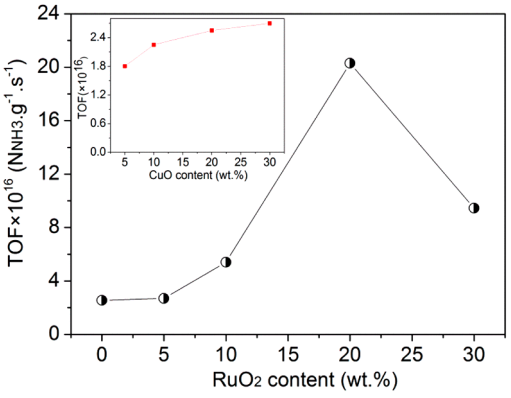

Figure 6. TOF value as a function of RuO_2 component amount for hierarchical pore *X*Ru20Cu/Al−ZrO_2 composites for NH_3 oxidation and the corresponding TOF plot for *X*Cu/Al−ZrO_2 composites in the inset.

(98 $m^2\ g^{-1}$)[23] and the conventional catalyst V_2O_5/TiO_2 (43.7 $m^2\ g^{-1}$),[9] which is also responsible for the high catalytic activity of 20Ru20Cu/Al−ZrO_2. Even for the Pd-supported ZSM-5 catalyst (4.1% Pd/ZSM-5) with a surface area of (330 $m^2\ g^{-1}$),[9] the NH_3 complete conversion temperature (300 °C) is 105 °C higher than that of 20Ru20Cu/Al−ZrO_2 (195 °C), although the N_2 selectivity is only 91% of the present 20Ru20Cu/Al−ZrO_2 catalyst.

Figure 8 gives the catalytic activity and the N_2 selectivity vs reaction temperature of the reference sample (20Ru/Al−ZrO_2 for NH_3) oxidation reaction. Although NH_3 can be completely

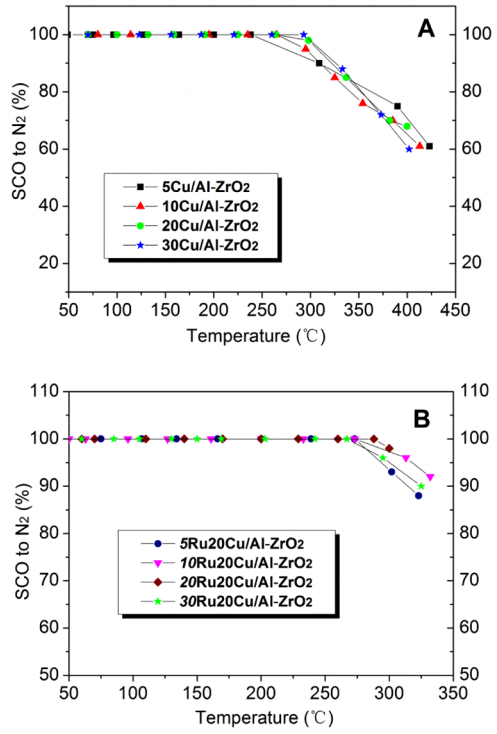

Figure 7. N_2 selectivity of NH_3 oxidation as a function of reaction temperature for hierarchical pore Cu/Al−ZrO_2 composites (A) and RuCu/Al−ZrO_2 composites (B).

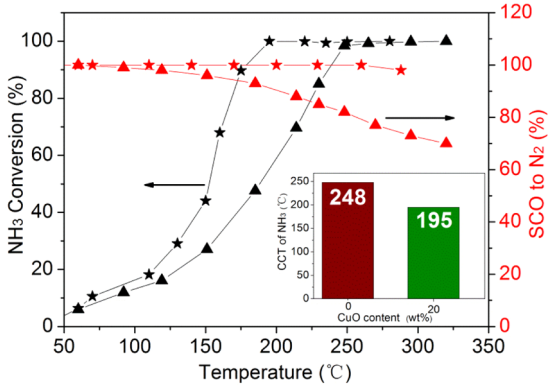

Figure 8. NH_3 conversion rate and N_2 selectivity as functions of reaction temperature for the reference sample 20Ru/Al−ZrO_2 without CuO loaded, (-▲-, 20Ru/Al−ZrO_2; -★-, 20Ru20Cu/Al−ZrO_2).

oxidized at 248 °C, its N_2 selectivity (82%) is much lower than that of 20Ru20Cu/Al−ZrO_2 (100%) at the temperature. Moreover, the N_2 selectivities of 20Ru/Al−ZrO_2 in the whole temperature range of the reaction are also lower than those of RuO_2 and CuO coloaded as composite 20Ru20Cu/Al−ZrO_2 and the *X*Cu/Al−ZrO_2 composite catalysts, suggesting the important role of the CuO component in enhancing the N_2 selectivity during the NH_3 oxidation reaction.

The catalytic activities of NH_3 SCO over reference samples 20Cu/ZrO_2 and 20Ru20Cu/ZrO_2 without Al doping are shown in Figure 9. NH_3 can be oxidized completely at 430 and 250 °C on the 20Cu/ZrO_2 and 20Ru20Cu/ZrO_2, respectively, with corresponding N_2 selectivities of 50% and 98%. The complete NH_3 oxidation temperature is much higher than that of 20Cu/Al−ZrO_2 (380 °C) and 20Ru20Cu/Al−ZrO_2 (195 °C), and the N_2 selectivity is lower compared with 20Cu/Al−ZrO_2

dx.doi.org/10.1021/cs500421x | ACS Catal. 2014, 4, 2195−2206

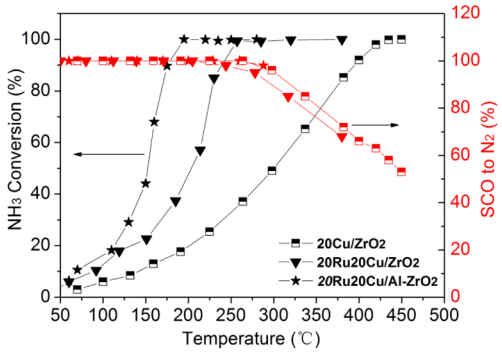

Figure 9. NH_3 conversion rate and N_2 selectivity as functions of reaction temperature for the reference samples $20Cu/ZrO_2$ and $20Ru20Cu/ZrO_2$ without Al doped.

(70%) and $20Ru20Cu/Al{-}ZrO_2$ (100%). This indicates that Al-doped hierarchically porous ZrO_2 can assist the $20Ru20Cu/Al{-}ZrO_2$ composite in the ammonia SCO reaction.

3.2.3. Catalytic Induction Capability and Stability. To investigate the catalytic induction capability and stability of the hierarchically porous catalysts, Figure 10 gives the relation between the NH_3 oxidation percentage on catalysts and the time on-stream (TOS) at a fixed temperature of 200 °C. The catalytic induction capability was characterized by the time period needed to achieve a stable conversion for each catalyst at a temperature of 200 °C. For $20Cu/Al{-}ZrO_2$, activation of the catalyst took ~25 min and then reached the steady-state reaction stage, according to Figure 10B. After RuO_2 and CuO were coloaded, the activation time became shorter, and it took about 15, 10, 0, and 3 min for $5Ru20Cu/Al{-}ZrO_2$, $10Ru20Cu/Al{-}ZrO_2$, $20Ru20Cu/Al{-}ZrO_2$, and $30Ru20Cu/Al{-}ZrO_2$, respectively, to reach the steady-state reaction stages under a space velocity of 120 000 mL h^{-1} g_{cat}^{-1}. More importantly, it can also be seen from Figure 10A that each catalyst keeps a stable NH_3 conversion rate at the fixed temperature, and no deactivation in ammonia oxidation is observed for as long as 8 h. Even at 175 °C, sample $20Ru20Cu/Al{-}ZrO_2$ still shows a stable catalysis activity (NH_3 conversion of 89%) for the ammonia SCO reaction, and no obvious decrease at the end of the 8 h can be observed (shown in SI Figure S5). This indicates the excellent catalytic stability of the hierarchically porous $RuO_2CuO/Al{-}ZrO_2$ composite catalyst toward NH_3 oxidation, which is highly desirable as catalysts for the ammonia SCO reaction.

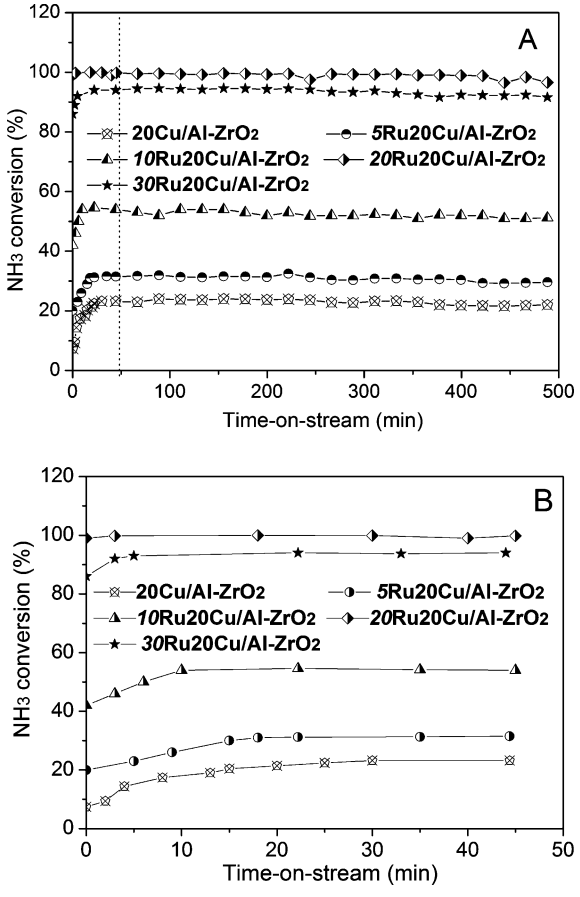

Figure 10. Time-on-stream behavior of NH_3 oxidation on hierarchically porous composite catalysts at 200 °C. Part B is the denoted time scales in part A.

4. DISCUSSION

4.1. Surface Chemical Compositions and Oxygen Vacancies. The catalytic activity of the catalysts is connected with the surface chemical composition. The surface compositional information on the prepared hierarchically porous composites collected by XPS and the results are shown in Figure 11. The XPS signals of Cu 2p (925−957 eV) in $Cu/Al{-}ZrO_2$ and $RuCu/Al{-}ZrO_2$ catalysts can be found in Figure 11A.

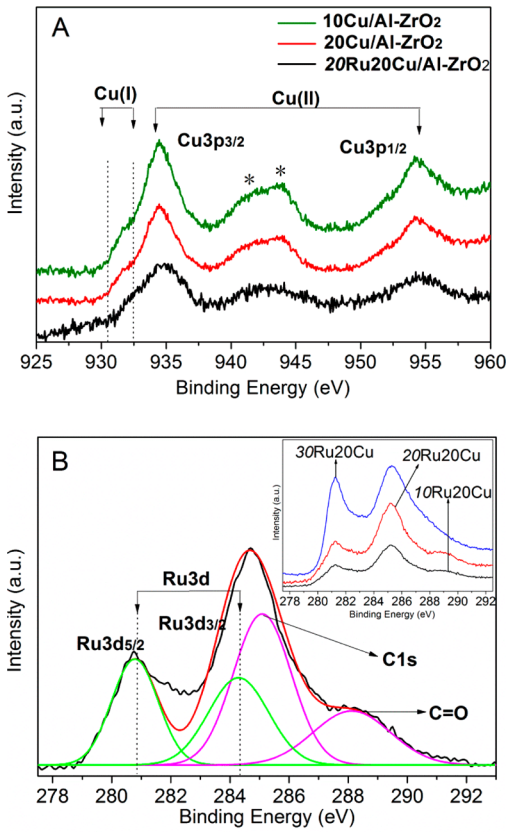

Figure 11. XPS spectra of Cu 2p (A), Ru 3d + C 1s (B) of sample $20Ru20Cu/Al{-}ZrO_2$. The inset in part B is the Ru 3d spectra of sample $10Ru20Cu/Al{-}ZrO_2$ (denoted as 10Ru20Cu), $20Ru20Cu/Al{-}ZrO_2$ (denoted as 20Ru20Cu), and $30Ru20Cu/Al{-}ZrO_2$ (denoted as 30Ru20Cu).

dx.doi.org/10.1021/cs500421x | ACS Catal. 2014, 4, 2195−2206

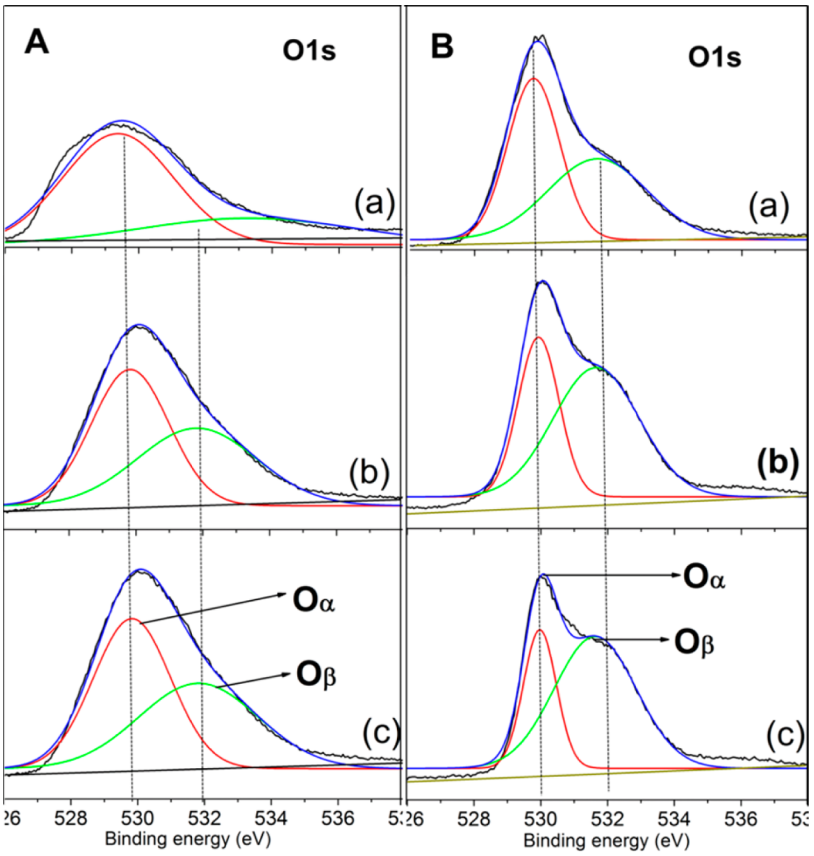

Figure 12. XPS spectra of O 1s of samples $RuCu/ZrO_2$ (A) and $RuCu/Al-ZrO_2$ (B). Parts a, b, and c in A are for ZrO_2, $20Cu/ZrO_2$, and $20Ru20Cu/ZrO_2$, respectively; a, b, and c in B are for $Al-ZrO_2$, $20Cu/Al-ZrO_2$, and $20Ru20Cu/Al-ZrO_2$, respectively.

The Cu $2p_{3/2}$ and Cu $2p_{1/2}$ peaks at around 934 and 954 eV, respectively, and the broadened one at 940−945 eV in the spectra can be attributed to Cu(II) ions in the form of CuO.[33,34] It can also be found that the main Cu $2p_{3/2}$ lines are broadened and asymmetric, which should be from Cu(I) species, suggesting that the Cu(I) species has been generated during calcination.[35] The couple of Cu^{2+}/Cu^{+} would contribute to the generation of oxygen vacancies in the prepared composite materials. Figure 11B shows the XPS spectra of Ru 3d + C 1s obtained from the hierarchically porous $20Ru20Cu/Al-ZrO_2$. The components at the binding energy positions of 281 and 284.2 eV can be well attributed to the Ru(IV) $3d_{5/2}$ and Ru(IV) $3d_{3/2}$ in RuO_2, respectively,[36] and the peak intensity at the binding energy 281 eV increases with the increase in the RuO_2 loading amount (the inset in Figure 11B). The components at the binding energy positions of 285 and 288.2 eV should be C 1s and C═O (or C−F) carbon species on the surface of the sample, respectively.

It can be seen from the XPS spectra of O 1s of the pure hierarchically porous ZrO_2, $Al-ZrO_2$, CuO, and $CuO-RuO_2$ loaded composite catalysts (Figure 12) that for all samples, the O 1s peaks comprise two overlapping peaks. The first peak, which has a lower binding energy of 529−530 eV, is attributed to the lattice oxygen (O_α).[37] The other overlapping peak of O 1s at binding energies of 532 eV is attributed to surface adsorbed oxygen (O_β).[38] The surface molar percentages and binding energies of O 1s in the hierarchically porous composite catalysts are summarized in Table 2. The results indicate that the molar ratio of O_β/O_T (O_T is the total rate of the O_α and O_β) increases from 11 to 30 after 20 wt % CuO is loaded onto ZrO_2 ($20Cu/ZrO_2$), and the percentage does not obviously increase after RuO_2 and CuO are coloaded on ZrO_2 ($20Ru20Cu/ZrO_2$).

Table 2. Surface Molar Percentages of O_α and O_β, and Binding Energies of O 1s of Hierarchically Porous Nanocomposites with Varied RuO_2 and CuO Loading Amounts

	binding energy (eV)		surface molar percent of O 1s (%)	
catalysts	O_α	O_β	O_α/O_T[a]	O_β/O_T[b]
$Al-lZrO_2$	529.8	531.8	67	31
$20Cu/Al-lZrO_2$	530	531.8	53	47
$20Ru20Cu/ZrAlO_x$	530	532	58	46
ZrO_2	529.3	533.5	89	11
$20Cu/ZrO_2$	529.8	532	70	30
$20Ru20Cu/ZrO_2$	529.9	531.9	64	33

[a]The ratio between O_α and O_T ($O_T = O_\alpha + O_\beta$). [b]The ratio between O_β and O_T ($O_T = O_\alpha + O_\beta$).

The $Al-ZrO_2$ series catalysts have the same trend (Figure 12B), in which the percentage of O_β in O_T increases from 31 ($Al-ZrO_2$) to 43 ($20Cu/Al-ZrO_2$) and reaches 47 ($20Ru20Cu/Al-ZrO_2$). This indicates that CuO addition can significantly increase the amount of surface adsorbed oxygen due to the coupling of Cu^{2+}/Cu^{+} (according to the XPS result in Figure 11A), which can produce oxygen vacancies, and the addition of RuO_2 has little effect on the surface adsorbed oxygen amount. On the other hand, it also can be found that the ratio of O_β/O_T in $Al-ZrO_2$, and $20Cu/Al-ZrO_2$ and

dx.doi.org/10.1021/cs500421x | ACS Catal. 2014, 4, 2195−2206

20Ru20Cu/Al−ZrO_2 composites, as well, is considerably higher than that in ZrO_2, suggesting that the Al doping in Al−ZrO_2 leads to the production of a high number of oxygen vacancies by the substitution of Al^{3+} for Zr^{4+}, which results in an increased amount of surface adsorbed oxygen. This result is consistent with the results reported by Chen et al.[39] and Lamaczet al.[40] In addition, Wu et al.[41] reported that the surface chemisorbed oxygen (O_β) is highly active during the oxidation reaction because of its higher mobility. Thus, the much enhanced performances of hierarchically porous 20Cu/Al−ZrO_2 and 20Ru20Cu/Al−ZrO_2 composites for NH_3 SCO reaction, as compared with Al-undoped 20Cu/ZrO_2 and 20Ru20Cu/ZrO_2 composites, respectively (Table 1, Figures 5 and 9), can be partially attributed to the increased amount of surface chemisorbed oxygen (O_β) (Table 2) produced by the Al doping in the ZrO_2 lattice.

4.2. Surface Activity of Metal Oxide Nanoparticles. The catalytic activities of the hierarchically porous composite surface were demonstrated by H_2-TPR, and the results are shown in Figure 13. Pure Al−ZrO_2 shows weak surface activity

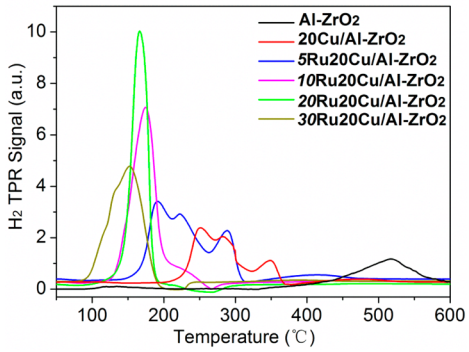

Figure 13. H_2-TPR profiles of the prepared hierarchically porous composites.

with its H_2-reduction peak at ~510 °C. After 20 wt % CuO addition, the redox activity of the obtained composite (20Cu/Al−ZrO_2) increases remarkably and shows three hydrogen consumption peaks at 350, 280, and 250 °C. The hydrogen consumption peaks at relatively low temperatures of 250 and 280 °C should correspond to the reductions of the surface-capped oxygen and the lattice oxygen due to the CuO nanoparticle loading, and that at the higher temperature should be due to the elimination of O^{2-} anions from the lattice in Al−ZrO_2. This is consistent with the report that the CuO addition can increase the surface activity of CeO_2 for the CuO/CeO_2 composite.[42,43] Attractively, the H_2-reduction peak of the hierarchically porous composite shifts to even lower temperatures after loading RuO_2, which are 190, 220, and 280 °C for 5Ru20Cu/Al−ZrO_2, around 60 °C lower than those of 20Cu/Al−ZrO_2. Moreover, the H-reduction peaks become stronger and shift to lower temperatures at increased RuO_2 addition amounts, that is, as shown, 180 °C for 10Ru20Cu/Al−ZrO_2, 170 °C for 20Ru20Cu/Al−ZrO_2, and 150 °C for 30Ru20Cu/Al−ZrO_2, meaning that a large amount of surface active species have been produced after the incorporation of RuO_2 nanoparticles into the hierarchically porous structure.

4.3. Synergetic Catalytic Effects among Metal Oxide Components for NH_3 SCO Reaction. The enhanced catalytic activity of the hierarchically porous RuO_2−CuO/Al−ZrO_2 composites for NH_3 SCO should be ascribed to the synergetic catalytic effects among the metal oxide composite. Shi[43] proposed the synergetic catalytic mechanism of bimetal oxide CuO/RuO_2 for ammonia SCO in a very systematic method named "successive catalytic functioning of two components in multistep reactions", and in this work, we will further discuss the role of the Al-doped ZrO_2 support in the SCO reactions. The NH_3 catalytic oxidation process on the hierarchically porous 20Ru20Cu/Al−ZrO_2 composite can be divided into four steps: (I) adsorption of reactant molecules, (II) NH_x (x = 1−3) dehydrogenations, (III) formation of the oxidation product, and (IV) desorption of the oxidation product.

RuO_2 is well-known as an active catalyst for the ammonia oxidation reaction; especially, the (110) surface of stoichiometric RuO_2 possesses numerous dangling bonds, exposing coordinatively unsaturated Ru_{cus} (Ru $1f_{cus}$) atoms, which are highly susceptive to NH_3 molecules.[20] In the adsorption process (Scheme 1A), the NH_3 and O_2 molecules can be

Scheme 1. Stick and Ball Model of the Stoichiometric RuO_2 (110) Surface[a]

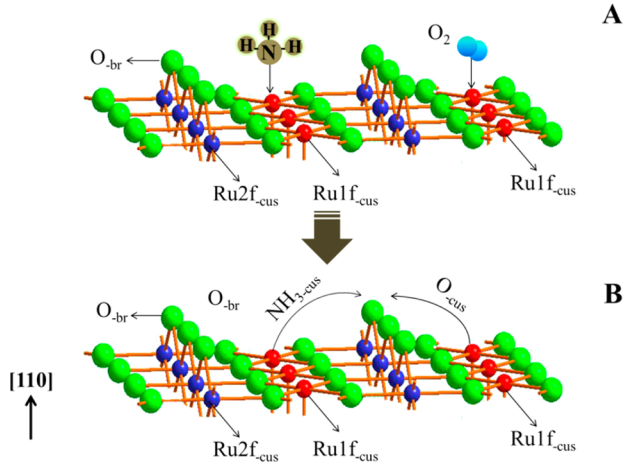

[a]Bridge oxygen (O_{br}) and Ru $1f_{cus}$ are 2-fold coordinated oxygen atoms and 5-fold coordinated Ru atoms, respectively. (A) NH_3 and O_2 molecules adsorbed on the Ru_{cus} sites competitively. (B) $NH_{3\text{-}cus}$ species are apt to react with O_{cus} to dehydrogenate.

competitively adsorbed onto these coordinatively unsaturated Ru_{cus} atoms to form $NH_{3\text{-}cus}$ and O_{cus} with the ΔE values of −1.36 and −1.21 eV, respectively, as shown in reactions 3 and 4. However, the adsorption of NH_3 molecules should be the more predominant because of the higher ΔE value.[24] For the hierarchically porous 20Ru20Cu/Al−ZrO_2 composite (Scheme 2), the Cu^{2+}/Cu^{+} coupling and the Al doping will generate a high number of oxygen vacancies in the hierarchically porous Al−ZrO_2 (reaction 5 and 6), according to the O 1s XPS result in Figure 12B and the high rate of O_β/O_T in Table 2, and the oxygen vacancies of the 20Ru20Cu/Al−ZrO_2 composite make O_2 molecules easily chemically adsorbed onto the surface of the catalyst to form active O* (Scheme 2), as reaction 7.[44]

$$NH_3(g) + Ru_{\text{-cus}} \rightarrow NH_{3cus} \qquad \Delta E = -1.36\ \text{eV} \tag{3}$$

$$O_2(g) + 2Ru_{cus} \rightarrow O_{2\text{-cus}} \rightarrow 2O_{cus} \qquad \Delta E = -1.21\ \text{eV} \tag{4}$$

$$CuO \rightarrow Cu(I)/Cu(II) + V\ddot{o} \tag{5}$$

dx.doi.org/10.1021/cs500421x | ACS Catal. 2014, 4, 2195−2206

Scheme 2. Schematic Illustrations of NH_3 and O_2 Molecules Adsorption on the Surface of Hierarchically Porous RuCu/Al−ZrO_2 Nanocomposite (left), and the Proposed Synergetic Catalytic Effect in Hierarchically Porous RuCu/Al−ZrO_2 Nanocomposite (right)[a]

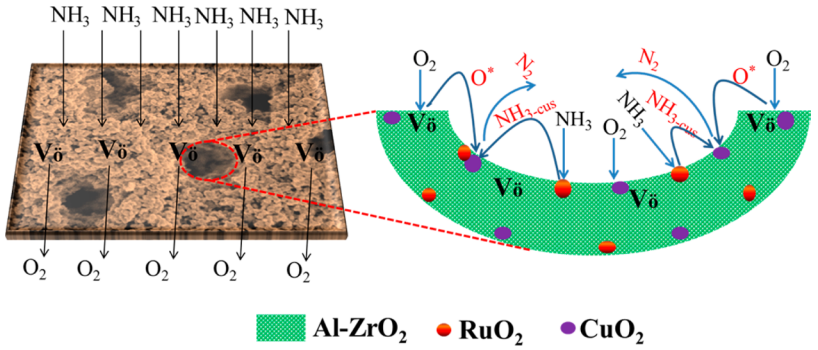

[a]Al−ZrO_2 matrix and the RuO_2 components first activate the oxygen and ammonia molecules into O* and $NH_{3\text{-cus}}$ by the large number of oxygen vacancies in the Al-doped matrix and the active (110) surface of RuO_2, respectively, then the adsorbed $NH_{3\text{-cus}}$ species on RuO_2 reacts with O*, leading to dehydrogenation of $NH_{3\text{-cus}}$ and the formation of $NO(N_xO_y)_{cus}$ or N_{cus} species. Finally, the $NO(N_xO_y)_{cus}$ intermediates are reduced to N_2 under the catalysis of CuO.

$$Al_2O_3 \rightarrow Al''_{Zr} + O_o^x + V\ddot{o} \quad (6)$$

$$O_2(g) + V\ddot{o} + 2e \rightarrow 2O^* \qquad \Delta E = -2.1\ \text{eV} \quad (7)$$

In the following dehydrogenation step, the formed $NH_{3\text{-cus}}$ species can react with either the O_{br} in the lattice of RuO_2 or the adsorbed active oxygen species (O_{cus}) on the surface of RuO_2, leading to the dehydrogenation and formation of intermediate $NH_{2\text{-cus}}$, NH_{cus}, and N_{cus} species (Scheme 1B). Compared with O_{br} in the lattice of RuO_2, the adsorbed $NH_{3\text{-cus}}$ species are apt to react with the O_{cus} species because the surface chemisorbed O_{cus} species is the activated oxygen species O*, which is highly active during the oxidation reaction.[41]

In the later oxidation process, the intermediates can react with each other to form $N_{2\text{-cus}}$, NO_{cus}, and other nitrogen oxide via reactions 8−11.

$$N_{cus} + N_{cus} \rightarrow N_{2\text{-cus}} + Ru_{cus} \quad (8)$$

$$N_{cus} + O_{cus} \rightarrow NO_{cus} + Ru_{cus} \quad (9)$$

$$NO_{cus} + O_{cus} \leftrightarrow NO_{2\text{-cus}} + Ru_{cus} \quad (10)$$

$$N_2O_{cus} + O_{cus} \rightarrow NO_{2\text{-cus}} + Ru_{cus} \quad (11)$$

$$NO_{cus} + NH_{2\text{-cus}} \xrightarrow{CuO} N_{cus} + H_2O \quad (12)$$

Copper oxide, especially CuO, is a special metal oxide that plays an important role in NH_3 catalytic oxidation reaction, and the copper ions in hierarchically porous Cu/Al−ZrO_2 and *X*Ru20Cu/Al−ZrO_2 composites exist as Cu(II), as shown from the XPS result in Figure 11A. The structure of CuO with Cu^{2+}−O^{2-} electronic transition species and the d−d transitions of Cu^{2+} in an octahedral environment with O*h* symmetry make it highly reduction-active in the ammonia conversion on the 20Ru20Cu/Al−ZrO_2 composite catalyst.[45] Thus, during the ammonia SCO reaction, the CuO component in the *X*Ru20Cu/Al−ZrO_2 composite is catalytically active in the reduction of nitrogen oxide into N_2 during ammonia oxidation,[12,19,46] which means that the intermediate NO-$(N_xO_y)_{cus}$ species adsorbed on the surface of RuO_2 can be reduced to N_2 selectively by CuO following reaction 12, leading to enhanced N_2 selectivity of the SCO, as evidenced in Figure 8. This is also consistent with the result reported by Ferrandon et al.[47] that the copper metal with fluorite-type oxide can be used to elucidate the reduction characteristics of carbon monoxide conversion.

The content of CuO in the catalyst is an important factor. A very low CuO content (e.g., <10% in the present case) in the *X*Cu/Al−ZrO_2 composites (Figures 5A and 7A) will be not effective enough in enhancing NH_3 oxidation activity and N_2 selectivity; however, a high amount of the CuO component (e.g., >20% in this case) may cover the active sites on the hierarchically porous Al−ZrO_2 surface to a large extent, leading to a slowing-down of adsorption of NH_3 and O species on the Al−ZrO_2 surface. The optimal CuO addition amount should be 20 wt % (*X*Cu/Al−ZrO_2) in the present case. After CuO and RuO_2 nanoparticles are coloaded in the Al−ZrO_2, both the N_2 selectivity and NH_3 conversion rate increase significantly, especially for the 20Ru20Cu/Al−ZrO_2 composite catalyst, owing to the easy adsorption of NH_3 and O species on the RuO_2 active surface, which results in the enhanced catalytic activity of the catalyst.

In the final desorption process, the $N_{2\text{-cus}}$ species on the surface of RuO_2 desorb and form N_2 gas, as shown in reaction 13, and the surface of Ru_{cus} is exposed again for further oxidation.

$$N_{2\text{-cus}} \rightarrow N_2(g) + Ru_{cus} \quad (13)$$

Therefore, the high and stable catalytic activity of the hierarchically porous 20Ru20Cu/Al−ZrO_2 oxide composite for the NH_3 SCO reaction can be understood on the basis of the synergetic catalytic effects among the oxides, in addition to the contribution by the hierarchically porous structure. In hierarchically porous Al−ZrO_2, a large number of oxygen vacancies are generated on the catalyst surface by the Al doping, which promotes the chemical adsorption of oxygen molecules and their activation to active oxygen species, O*, on surface. Meanwhile, NH_3 molecules are adsorbed on RuO_2. In this process, the Al−ZrO_2 matrix plays a synergetic role with RuO_2 in activating oxygen. Later, the reaction between the adsorbed $NH_{3\text{-cus}}$ and O* leads to the dehydrogenation of NH_3 and the formation of intermediates $NH_{2\text{-cus}}$, NH_{cus}, and N_{cus} species, and the generation of further oxidized intermediate NO. In the following stage, CuO functions as a catalyst for the reduction of NO (eq 12), which ensures the high selectivity to N_2 in the ammonia SCO, following a proposed successive catalytic

dx.doi.org/10.1021/cs500421x | ACS Catal. 2014, 4, 2195−2206

functioning mechanism.[43] At the fixed CuO loading amount (20 wt %), the optimum ratio of RuO_2/CuO is found to be 1:1, at which the NH_3 can be oxidized completely at 195 °C and 100% selectively to N_2 on the hierarchically porous 20Ru20Cu/Al−ZrO_2 composite. It is believed at such an optimum ratio between RuO_2 and CuO that the sequential reactions of NH_3 oxidation and elimination of the undesired intermediate NO can be optimally balanced.

5. CONCLUSIONS

A kind of highly efficient catalyst, a hierarchically porous RuO_2−CuO/Al−ZrO_2 composite with RuO_2 and CuO nanoparticles homogeneously dispersed in the porous structure of the support, has been successfully synthesized by the hydrothermal and wet impregnation method. The composite catalyst shows high and stable catalytic activity for ammonia SCO reaction, and NH_3 can be completely oxidized at 195 °C with 100% N_2 selectivity on the 20Ru20Cu/Al−ZrO_2 with a 1:1 RuO_2/CuO weight ratio. The high performance of the hierarchically porous RuO_2−CuO/Al−ZrO_2 composite catalyst is attributed to the synergetic catalytic effects among the transition metal oxides, in which the Al−ZrO_2 matrix and the RuO_2 components first activate the oxygen and ammonia molecules into O* and $NH_{3\text{-cus}}$ by the large number of oxygen vacancies in the Al-doped matrix and the active (110) surface of RuO_2, respectively. Subsequently, the CuO plays a successive role of catalyzing the NO reduction, an undesired intermediate during the $NH_{3\text{-cus}}$ oxidation by O*, into N_2.

■ ASSOCIATED CONTENT

Supporting Information

N_2 sorption and pore size distribution curves of samples *X*Cu/ZrO_2, the characterizations of reference samples (ZrO_2, 20Cu/ZrO_2, and 10Ru20Cu/ZrO_2), including XRD, SEM, TEM, and performance test. This material is available free of charge via the Internet at http://pubs.acs.org.

■ AUTHOR INFORMATION

Corresponding Author

*Phone: 86-21-52412714. Fax: 86-21-52413122. E-mail: jlshi@mail.sic.ac.cn.

Notes

The authors declare no competing financial interest.

■ ACKNOWLEDGMENTS

We gratefully acknowledge the financial support from the National Key Basic Research Program of China (2013CB933200), National Natural Science Foundation of China (51202278), Key Program for Science and Technology Commission of Shanghai Municipality (11JC1413400), and National Natural Science Foundation of Shanghai (12ZR1435200).

■ REFERENCES

(1) Amblard, M.; Burch, R.; Southward, B. W. L. *Appl. Catal., B* **1999**, *22*, L159−L166.
(2) Long, R. Q.; Yang, R. T. *J. Catal.* **2001**, *201*, 145−152.
(3) Gang, L.; van Grondelle, J.; Anderson, B. G.; van Santen, R. A. *J. Catal.* **1999**, *186*, 100−109.
(4) Huang, C. M. *J. Hazard. Mater.* **2010**, *180*, 561−565.
(5) Olofsson, G.; Hinz, A.; Andersson, A. *Chem. Eng. Sci.* **2004**, *59*, 4113−4123.
(6) Lippits, M. J.; Gluhoi, A. C.; Nieuwenhuys, B. E. *Catal. Today* **2008**, *137*, 446−452.
(7) Zhang, L.; He, H. *J. Catal.* **2009**, *268*, 18−25.
(8) Hong, S.; Karim, A.; Rahman, T. S.; Jacobi, K.; Ertl, G. *J. Catal.* **2010**, *276*, 371−381.
(9) Li, Y.; Armor, J. N. *Appl. Catal., B* **1997**, *13*, 131−139.
(10) Amores, J. M. G.; Escribano, V. S.; Ramis, G.; Busca, G. *Appl. Catal., B* **1997**, *13*, 45−58.
(11) Chmielarz, L.; Kustrowski, P.; Lasocha, A. R.; Dziembaj, R. *Appl. Catal., B* **1997**, *58*, 235−244.
(12) Gang, L.; Grondelle, J. V.; Anderson, B. G.; Santen, R. A. V. *J. Catal.* **1999**, *186*, 100−109.
(13) Lietti, L.; Ramis, G.; Busca, G.; Bregani, F.; Forzatti, P. *Catal. Today* **2000**, *61*, 187−195.
(14) Lee, J. Y.; Kim, S. B.; Hong, S. C. *Chemosphere* **2003**, *50*, 1115−1122.
(15) Wang, Z.; Qu, Z.; Quan, X.; Wang, H. *Appl. Catal., A* **2012**, *411*, 131−138.
(16) Shan, W.; Liu, F.; He, H.; Shi, X.; Zhang, C. *Appl. Catal., B* **2012**, *115*, 100−106.
(17) Wang, Z.; Qu, Z.; Quan, X.; Li, Z.; Wang, H.; Fan, R. *Appl. Catal., B* **2013**, *134*, 153−166.
(18) Lee, S. M.; Lee, H. H.; Hong, S. C. *Appl. Catal., A* **2014**, *115*, 100−106.
(19) Hung, C. M. *J. Hazard. Mater.* **2009**, *166*, 1314−1320.
(20) Wang, Y.; Jacobi, K.; Schöne, W. D.; Ertl, G. *J. Phys. Chem. B* **2005**, *109*, 7883−7893.
(21) Wang, C.-C.; Yang, Y.-J.; Jiang, J.-C.; Tsai, D.-S.; Hsieh, H.-M. *J. Phys. Chem. C* **2009**, *113*, 17411−17417.
(22) Perez-Ramirez, J.; Lopez, N.; Kondratenko, E. V. *J. Phys. Chem. C* **2010**, *114*, 16660−16668.
(23) Cui, X.; Zhou, J.; Ye, Z.; Chen, H.; Li, L.; Ruan, M.; Shi, J. *J. Catal.* **2010**, *270*, 310−317.
(24) Wang, C. C.; Wu, J.-Y.; Pham, T. L. M.; Jiang, J.-C. *ACS Catal.* **2014**, *4*, 639−648.
(25) Zweidinger, S.; Hofmann, J. P.; Balmes, O.; Lundgren, E.; Over, H. *J. Catal.* **2010**, *272*, 169−175.
(26) Hevia, M. A. G.; Amrute, A. P.; Schmidt, T.; Pérez-Ramírez, J. *J. Catal.* **2010**, *276*, 141−151.
(27) Over, H.; Kim, Y. D.; Seitsonen, A. P.; Wendt, S.; Lundgren, E.; Schmid, M.; Varga, P.; Morgante, A.; Ertl, G. *Science* **2000**, *287*, 1474−1476.
(28) Liu, Z. P.; Hu, P.; Alavi, A. *J. Chem. Phys.* **2001**, *114*, 5956−5957.
(29) Madje, B. R.; Patil, P. T.; Shindalkar, S. S.; Benjamin, S. B.; Shingare, M. S.; Dongare, M. K. *Catal. Commun.* **2004**, *5*, 353−357.
(30) Ramu, S.; Lingaiah, N.; Prabhavathi Devi, B. L. A.; Prasad, R. B. N.; Suryanarayana, I.; Sai Prasad, P. S. *Appl. Catal., A* **2004**, *276*, 163−168.
(31) Kozlowski, J. T.; Behrens, M.; Schlogl, R.; Davis, R. J. *ChemCatChem.* **2013**, *5*, 1989−1997.
(32) Das, S. K.; El-Safty, S. A. *ChemCatChem.* **2013**, *5*, 3050−3059.
(33) Bera, P.; Priolkar, K. R.; Sarode, P. R.; Hegde, M. S.; Emura, S.; Kumashiro, R.; Lalla, N. P. *Chem. Mater.* **2002**, *14*, 3591−3601.
(34) Tschöpe, A.; Trudeau, M. L.; Ying, J. Y. *J. Phys. Chem. B* **1999**, *103*, 8858−8863.
(35) Hartmann, P.; Brezesinski, T.; Sann, J.; Lotnyk, A.; Eufinger, J.-P.; Kienle, L.; Janek, J. *ACS Nano* **2013**, *7*, 2999−3013.
(36) Villullas, H. M.; Mattos-Costa, F. I.; Bulhões, L. O. S. *J. Phys. Chem. B* **2004**, *108*, 12898−12903.
(37) Avgouropoulos, G.; Loannides, T. *Appl. Catal., B* **2006**, *67*, 1−11.
(38) Xia, Y. S.; Dai, H. X.; Zhang, L.; Deng, J. G.; He, H.; Au, C. T. *Appl. Catal., B* **2010**, *100*, 229−237.
(39) Chen, L.; Li, J.; Ge, M. *J. Phys. Chem. C* **2009**, *113*, 21177−21184.
(40) Lamacz, A.; Krzton, A.; Mariadassou, G. D. *Catal. Today* **2011**, *176*, 347−351.

(41) Wu, Z.; Jin, R.; Liu, Y.; Wang, H. *Catal. Commun.* **2008**, *9*, 2217−2220.
(42) Avgouropoulos, G.; Ioannides, T. *Appl. Catal., A* **2003**, *224*, 155−167.
(43) Shi, J. *Chem. Rev.* **2013**, *113*, 2139−2181.
(44) Yang, Z. X.; Woo, T. K.; Baudin, M.; Hermansson, K. *J. Chem. Phys.* **2004**, *120*, 7741−7749.
(45) de Carvalho, M. C. N. A.; Passos, F. B.; Schmal, M. *Appl. Catal., A* **2000**, *193*, 265−276.
(46) Hung, C. M. *Powder Technol.* **2009**, *196*, 56−61.
(47) Ferrandon, M.; Ferrand, B.; Björnbom, E.; Kliingstedt, F.; Neyestanaki, A. K.; Karhu, H.; Väyrynen, J. *J. Catal.* **2001**, *202*, 354−366.